IEEE Access
Multidisciplinary ⋮ Rapid Review ⋮ Open Access Journal

Received 7 September 2022, accepted 7 November 2022, date of publication 10 November 2022,
date of current version 16 November 2022.

Digital Object Identifier 10.1109/ACCESS.2022.3221407

RESEARCH ARTICLE

Color Correction and Local Contrast Enhancement for Underwater Image Enhancement

SONGLIN JIN[1], PEIXIN QU[1], YING ZHENG[1], WENYI ZHAO[2], AND WEIDONG ZHANG[1]
[1]School of Information Engineering, Henan Institute of Science and Technology, Xinxiang 453003, China
[2]School of Artificial Intelligence, Beijing University of Posts and Telecommunications, Beijing 100876, China

Corresponding author: Weidong Zhang (zwd_wd@163.com)

This work was supported in part by the Natural Science Foundation of Henan Province under Grant 212300410345; in part by the Key Specialized Research and Development Program of Science and Technology in Henan Province under Grant 202102210388, Grant 212102110298, and Grant 222102210171; and in part by the Ministry of Education of China Industry-University Cooperation Collaborative Education Project under Grant 202002259018, Grant 202102256003, and Grant 202102256011.

ABSTRACT Underwater images suffer from various quality degradation problems such as color cast, low contrast, and blurred details. To solve these issues, a novel underwater image enhancement method that can implement color correction, detail sharpening, and contrast enhancement in stages. In particular, the proposed method combines multi-channel color compensation with color correction. It solves detail blurring and low contrast by the Gaussian differential pyramid and the local contrast enhancement of contrast limited adaptive histogram equalization, respectively. The proposed method mainly includes color compensation, color correction, detail sharpening, and contrast enhancement. Qualitative and quantitative comparisons demonstrate that the proposed method can effectively remove the blur of the image, realize the color correction, and significantly improve the clarity of the image.

INDEX TERMS Underwater image enhancement, color correction, detail sharpening, contrast enhancement.

I. INTRODUCTION

The ocean is bred with abundant resources. With the expansion of population and the scarcity of land resources, the demand for the development of marine resources is becoming increasingly urgent. Collecting marine information is the premise of developing and utilizing marine resources. Image is an important means for a human to obtain information, and underwater optical imaging has become the focus of attention. It plays an important role in marine resource exploration [1], marine ecological research [2], marine automatic monitoring [3], underwater target tracking [4], and underwater autonomous navigation [5]. However, the complex and changeable underwater environment, make underwater imaging generally suffer from very serious degradation phenomena, including atomization color distortion, etc. These problems have a serious impact on the acquisition of image information. These problems have a serious impact on the acquisition of image information. Therefore, how complete the restoration of underwater images by technical means, so as to obtain unambiguous underwater images, plays an important role in ocean exploration. An effective method that can enhance underwater images with better clarity, higher contrast, more detail, and full colors, which can provide the necessary safeguards for a variety of complex underwater applications [1], [2], [3], [4], [5].

In this paper, we propose a new underwater image enhancement method that can obtain more realistic underwater images. Firstly, color compensation is implemented for the original image and then color corrected using multi-scale Retinex. Secondly, the Gaussian differential pyramid is used to reconstruct and fusion of detailed information. Finally, the CLAHE is used to stretch the contrast of the detail-sharpened image. In this way, a high-quality underwater image is an output. Subjective and objective performance analysis, runtimes, and local feature point matching are used to evaluate the method. The experimental results show that the enhanced underwater images have higher contrast, brightness, and more detail and color than several methods. The main contributions of this paper are summarized as follows:

The associate editor coordinating the review of this manuscript and approving it for publication was Jeon Gwanggil.

1) An underwater image enhancement method is proposed based on color correction and local contrast enhancement. Compared with the state-of-the-art underwater image restoration or enhancement methods, the proposed method can effectively improve the quality of underwater images and reduce detail information loss without implementing color space transformation.

2) Considering that the degradation of underwater images is caused by the attenuation of light with different wavelengths, it is essential for color compensation for red and blue channels. The Multi-Scale Retinex (MSR) method based on auto-levels is implemented to effectively correct the compensated underwater image's color cast.

3) To highlight the details of the color-corrected image, the detail feature map of the R, G, and B channels are reconstructed using the Gaussian differential pyramid and fused into the R, G, and B channels corresponding to the color-corrected image.

4) To further improve the contrast of the underwater image, the pixel values of the high, medium, and low intervals are processed using CLAHE. Finally, the pixel values of the high and low intervals are effectively suppressed, and the pixel values of the middle interval are effectively stretched.

The specific arrangement of the remaining sections is as follows: Section II introduces several image enhancement methods. Section III presents the details of our proposed method. Section IV compares and analyzes the experimental results. Section V summarizes the work of this paper and future research.

II. RELATED WORK

Collecting high-quality image information in a complex underwater environment is challenging, so the image enhancement technique has been extensively studied [6], [7] to meet the needs of practical applications. Restoration parameters are derived from physical models and prior knowledge, restoring high-quality underwater images [8]. The non-physical model method obtains underwater images with rich information and better visuals [9] by adjusting the pixel values of the original image.

The methods based on the physical model mainly include specialized hardware, multiple images, and prior knowledge. Although these methods use specialized hardware [10], [11], [12], [8], although the technology has particular effectiveness in enhancing and restoring underwater images, it still has some limitations. For instance, the underwater optical imaging system is complex and expensive because of using complex hardware acquisition devices (e.g., optical laser sensor) to capture turbid underwater images.

For the second class of methods using multiple images [13], [14], [15] or approximate estimation of the scene [16], [17]. Narasimhan et al. [13] and Schechner et al. [14] employed multiple images for underwater image restoration, but it needs to use more than two images of the same scene as a priori knowledge, which will limit the real-time performance of video observations. Treibitz et al. [15] take into account the partial polarization of object reflection and backscattering from more than two images, but the process of image acquisition is complicated. Kopf et al. [16] used the existing geospatial information and the urban 3D models to restore images, but some additional information needs to be provided by user interaction. Tian et al. [17] used synthetic aperture imaging and polarization imaging to restore images, which could effectively increase the amount of information obtained by a single imaging system. However, it requires more complex hardware systems, thereby it isn't suitable for ordinary users.

For the third class of methods using prior knowledge [18], [19], [20], [21], [22]. The dark channel prior (DCP) proposed by He et al. [18] is used for outdoor image dehazing. Image degradation in foggy and underwater is caused by scattering and absorption of media, thereby the method can be used for image restoration [19], [20], [21], [22].

The non-physical models are mainly divided into five categories: transform domain-based method, spatial domain-based method, color constancy-based method, deep learning method, and fusion method. For the first class of methods mainly includes quaternion [23], homomorphic filter [24], and wavelet transform [25]. This kind of method has a good effect on noise removal, but it can't achieve ideal results in contrast and color of underwater images.

The spatial domain-based methods mainly include grayscale transformation [26], histogram equalization (HE) [27], and contrast limited adaptive histogram equalization (CLAHE) [28]. The HE stretches the histogram evenly globally to improve the image contrast [29]. However, HE increases the sparsity of the gray distribution of the image, which may lose part of the detailed information. Adaptive histogram equalization (AHE) [30] improves the local contrast of the image and enhances edge details by redistributing the local gray level of the image multiple times, but it also has the problem of amplifying noise. Based on the AE, CLAHE imposes constraints on the local image contrast to avoid excessively amplifying image noise in enhancing image contrast. Hitam et al. [31] proposed a comprehensive CLAHE color model and applied the CLAHE method to the RGB and HSV color models, respectively.

For the third class of methods mainly includes White Balance [32], Gray World [33], Gray Edge [34], Weighted Grey Edge [35], and Retinex [36]. White balance may cause color distortion when there is insufficient light. Blurred edges of underwater images due to the complexity of the underwater environment, the results are not ideal when the assumed conditions of Gray World, Gray Edge, and Weighted Grey Edge are destroyed. Joshi et al. [37] applied Retinex to weather degraded images, but its enhancement effect is limited. Based on the Retinex theory, Fu et al. [38] reposed to use different methods to enhance the two components of incident and reflection of underwater images. They achieved a good enhancement effect in the case of color deviation in underwater images. Alex et al. [39] converted the image to the YCbCr color space and achieved good enhancement effects.

Deep learning was gradually emerging and applied in various fields, and underwater image enhancement [40], [41], [42], [43], [44], [45], [46] is no exception. Perez et al. [40] used a convolutional neural network (CNN) for image enhancement for the first time. This method uses the correspondence between degraded underwater images and clear images to train a model between image pairs to achieve the purpose of underwater image enhancement. Zhang et al. [41] proposed an enhancement method based on Retinex-inspired color correction and detail-preserved fusion to accomplish the color correction of underwater images and enhance image edges and details. Zong et al. [42] proposed an enhancement algorithm based on CycleGAN to enhance the robustness and adaptability of the network. Zhang et al. [43] suggested using color correction and Bi-interval contrast enhancement to improve the quality of underwater images. Sun et al. [44] proposed an enhancement method based on reinforcement learning. This method uses a Markov decision process for modeling to enhance the underwater image. Liu et al. [45] proposed an object-guided twin adversarial contrastive learning to enhance the underwater image. Wang et al. [46] suggested using the CA-GAN method for image enhancement. First, underwater degraded images with different attenuation coefficients and depths are synthesized according to the physical model, and then CA-GAN is used to create a many-to-one mapping function, and an attention mechanism is also introduced to improve the visual effect of the image. However, deep learning relies heavily on training data and hardware. Therefore, it is not available to all users.

Ancuti et al. [47] first proposed a fusion method in 2012. In 2018, Ancuti et al. [48] improved the model and achieved better enhancement effects. However, the fusion weighting coefficient of this method is challenging to determine, and the fusion image has local over-enhancement or under-enhancement. Sethi et al. [49] attempted to fuse physical and non-physical models and obtained an excellent enhancement effect by Laplacian pyramid fusion after the underwater images were processed via HE and DCP dehazing, respectively. Liu et al. [50] proposed an enhanced model based on CGAN, which fuses global and local features at each scale, reducing unnecessary artifacts.

Although Ancuti et al. [48] enhance the quality of images effectively, it introduces too many fusion images and weights. In contrast, our method does not change the color space without introducing too many fusion weights. It processes degraded underwater images by color compensation, color correction, detail sharpening, and local contrast enhancement. Besides, our extensive experiments reveal that our method has better subjective and objective evaluation. To ensure high efficiency, it can also improve the accuracy of the key point matching method.

III. PROPOSED METHOD

As shown in Fig. 1, our method consists of four main parts: color compensation, color correction, detail sharpening, and local contrast enhancement. Details of the four vital operations are presented in subsequent sections. Where the detailed flow of detail sharpening is shown in Fig. 5.

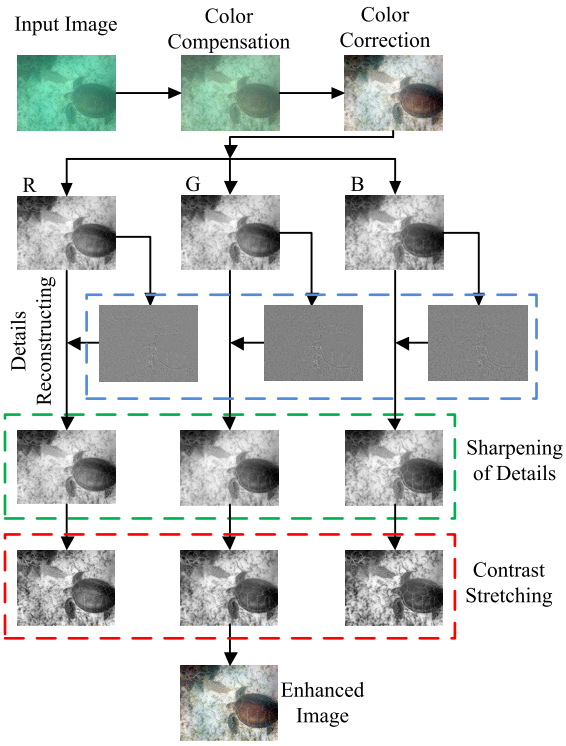

FIGURE 1. The framework of the proposed method.

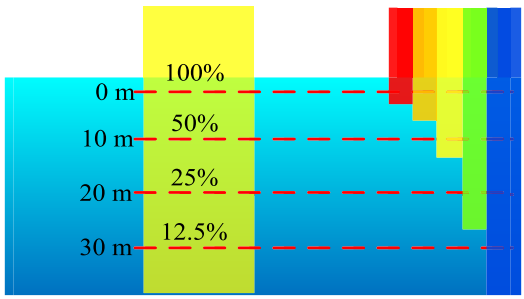

FIGURE 2. Selective attenuation of light of different wavelengths underwater.

A. COLOR COMPENSATION

Light decays when propagating underwater [51], resulting in poor-quality of images [52]. The attenuation of the underwater color is detailed as depicted in Fig. 2. It can observe that the wavelength of red light has the longest attenuation and the shortest transmission distance. In contrast, the wavelength of blue (green) light has a shorter attenuation and a longer transmission distance. These objective facts will result in images captured underwater generally rendered green-bluish appearance. It can be concluded that the value of the red channel is much smaller than the other two-color channels. Red channels tend to be overcompensated when color correction is performed directly.

FIGURE 3. Comparison before and after color compensation: 1. The first row is original image; 2. The second row is color compensated underwater images.

Thus, we first compensate the original image with the red channel before performing color correction. Mathematically, the compensation for the red channel is defined as follows:

$$I_{rc}(x) = I_r(x) + \alpha.(\bar{I}_g - \bar{I}_r).(1 - I_r(x)).I_g(x) \quad (1)$$

where $I_r(x)$ represent the red channel, $I_g(x)$ represent the green channel, $\bar{I}_r$ represent the average values of $I_r(x)$, $\bar{I}_g$ represent the average values of $I_g(x)$, and α represents constant parameters. Considering the red channel attenuation is strong. Finally, extensive experiments determine that the value of α is set to 1.5 with a better compensating effect.

The blue channel may also show significant attenuation in a water environment with more plankton or organic matter. Then the compensation of the blue channel can be expressed as:

$$I_{bc}(x) = I_b(x) + \alpha.(\bar{I}_g - \bar{I}_b).(1 - I_b(x)).I_g(x) \quad (2)$$

where $I_b(x)$ represent the blue channel, $I_g(x)$ represent the green channel, $\bar{I}_b$ represent the average values of $I_b(x)$, $\bar{I}_g$ represent the average values of $I_g(x)$, and α represents constant parameters, the compensation factor α of the blue is set to 1.0.

Fig. 3 shows the underwater images before and after color compensation. The overall visual effect of degraded underwater images is improved, and green color is effectively suppressed by color compensation. From left to right, the result of color compensation is better when the green color of the degraded image is more obvious. However, the compensated images still suffer from blurred details and color distortion. We will focus on the blur of detail in section B.

IV. COLOR CORRECTION

This section uses a multi-scale Retinex [38], [53] to complete the color correction. In the visual perception of human eyes, the application of color constancy theory enables human eyes to adapt to different lighting conditions. In recent years, multi-scale Retinex with color restoration (MSRCR) has introduced color correction for each channel to effectively suppress the problems associated with MSR-enhanced images [54].

The visible light image consists of two parts: illumination and reflection, so it can be defined as:

$$\log(S(x,y)) = \log(L(x,y)) + \log(R(x,y)) \quad (3)$$

where $S(x,y)$ represents the visible light image, and $L(x,y)$ represents the illumination, $R(x,y)$ represents reflection. In order to obtain more accurate reflection components of $S(x,y)$, we convolve $S(x,y)$ with Gaussian kernel functions. Therefore, the reflection component can be defined (4), as shown at the bottom of the next page, where $c \in \{R, G, B\}$ corresponds to three color channels of R, G and B, $MSR_c(x,y)$ represents the output image corresponding to the c^{th} channel, N represents the number of Gaussian functions corresponding to different standard deviations, w_n represents the weight for each output image, where $w_1 + w_2 + \cdots + w_n = 1$, and σ is the standard deviation. Typically, $\sigma \in \{\sigma_1, \sigma_2, \sigma_3, \sigma_4, \sigma_5, \sigma_6\}$ is the vector of Gaussian fuzzy coefficients, $0 \le \sigma_1 < \sigma_2 < 50$ are two small scales, $50 \le \sigma_3 < \sigma_4 < 100$ are two medium scales, and $100 \le \sigma_5 < \sigma_6$ are two large scales.

We have already given the validity of MSRCR application to some images with thick fog for color correction in [55]. We applied MSRCR to the underwater image in the third row of Fig. 4, and we find that although MSRCR improved color and contrast, it brought about the phenomenon of detail loss and reddishness. By observing the tricolor histogram and the MSRCR corrected images and comparing the probability of their corresponding 0-pixel value, the probability of the 0-pixel value of G and B channels increased significantly after MSRCR correction, while the probability of the 0-pixel value of the R channel decreased significantly. Therefore, the probability increases of the 0-pixel value of MSRCR-corrected images is the leading cause of the blurring of details. In addition, we found that the tricolor histograms of most enhanced images are distributed in the middle region, and a few images are distributed in the right area.

In summary, we propose an auto-level-based MSR color correction method to address the blurring of details and color distortion of images.

Firstly, the gray histogram of R, G, and B channels is calculated using auto-levels. Then, the highlight value and shadow value of R, G, and B channels are determined by clipping proportion and used as clipping boundary. Finally, the same linear stretch is applied to the middle part of each channel, and each gray value is ensured to be in the interval [0, 255]. Therefore, the expression of linear stretch is (5), as shown at the bottom of the next page, where $MSRCR_c(x,y)$ represents the gray value after color correction, $Min = I\_Sort(m * n * per)$ and $Max = I\_Sort(m * n * (1 - per))$ represent the lower and upper limits of clipping boundary, m represent the rows, n represent the columns, I_Sort represents the matrix of the

sorted grayscale values and $I\_Sort = Sort\,(MSR_c)$, and per is the proportion of clipping and is set to 0.5% by extensive experiments.

Fig. 4 shows that red artifacts and color distortion still appear in local areas of the image with the MSRCR-based color correction method. Therefore, we propose reconstructing the detail and edge information using the Gaussian difference pyramid and fuse it into the color-corrected image to highlight the details of the image in section C.

A. DETAIL SHARPENING

The finer the scale, the more image detail increases, and the course the scale, the more image detail is lost. On this basis, the multi-scale space is built to describe the image feature information changing with the scale. More multi-scale spatial representation sequences are obtained by introducing the continuous variation parameters of the scale. The scale spaces are extracted from these sequences to realize the feature extraction at different resolutions. Pyramid transformation has been gradually applied to image defogging [56], image classification [57], and underwater image enhancement [47], [48] due to its good performance in feature extracting and edge-preserving.

An enhanced underwater image with blurred details in section C, thereby this section main considers the reconstruction of detailed information. We firs get the Retinex enhanced image I_1, and then the details of the R, G, and B channels are taken by three steps of decomposition, differential, and reconstruction of the Gaussian pyramid. Finally, the reconstructed details and image I_1 are fused to get image I_2, as shown in Fig. 5.

Decomposition process of Gaussian pyramid transformation: first define Gaussian kernel w_k with k different scales and different window sizes, and then use w_k to implement convolution operation with the original image I_1 to get k image of same size G_0, and G_0 as the 0^{th} layer of the k^{th} Gaussian pyramid. Similarly, the construction method of the image G_l^k in the l^{th} layer of the k^{th} Gaussian pyramid: the image G_{l-1}^k of the $(l-1)^{th}$ layer and the Gaussian kernel w_k are convolved, and the convolution result is subjected to binary extraction in the row and column directions. G_l^k is expressed as follows:

$$\begin{cases} G_l^k\,(i,j) = \sum\limits_{m_k=-2}^{2}\sum\limits_{n_k=-2}^{2} w_k\,(m_k,n_k,\sigma_k)\,G_{l-1}^k \\ \qquad\qquad (2x+m_k,\,2y+n_k) \\ (1 \le l \le N, 0 \le i \le R_l, 0 \le j \le C_l) \end{cases} \tag{6}$$

where N is the maximum number of layers, R_l denotes the number of rows of the lth layer image, C_l denotes the number of columns of the lth layer image. The size of the image G_l^k of the l^{th} layer of the Gaussian pyramid is four times smaller compared to G_{l-1}^k. We construct two Gaussian pyramids G_l^1 and G_l^2 when $k = 2$, w_1 is a Gaussian kernel with a scale and radius of 3, and w_2 is a Gaussian kernel with a scale and radius is 5.

Two Gaussian pyramids G_l^1 and G_l^2 with the same number of layers are obtained by Eq. (6). The small-scale image obtained by the decomposition contains rich image details. The detail of large-scale image is significantly reduced, which mainly including contour information and with better noise immunity. The analysis found that combining the advantages of both is beneficial to the preservation of details and contour information. The Gaussian differential pyramid can be obtained by the differential of adjacent images of each layer of the Gaussian pyramid. The construction method of D_l as:

$$D_l\,(i,j) = G_l^1\,(i,j) - G_l^2\,(i,j) \tag{7}$$

Based on Eq. (7), double up-sampling is performed from the lth layer to the first layer, and then the images up sampled on this layer are accumulated to the upper layer, and this operation is repeated until it is accumulated to the 0^{th} layer. Finally, the reconstructed expression of detail information can be defined as:

$$I_d\,(i,j) = \sum_{l-1}\{D_{l-1}\,(i,j) + U\,(D_l\,(i,j))\} \tag{8}$$

where I_d is the reconstructed detail image and $U\,(D_l\,(i,j))$ is the double up-sampling operation on the image of the l^{th} layer. In summary, the reconstructed detail information I_d

$$\begin{cases} MSR_c\,(x,y) = \sum\limits_{n=1}^{N} w_n\,\{\log(S_c\,(x,y)) - \log(G_n\,(x,y) * S_c\,(x,y))\} \\ G_n\,(x,y) = \dfrac{1}{2\pi\sigma_n^2}\exp\dfrac{-\left((x-x\_center_w)^2 + (y-y\_center_w)^2\right)}{2\sigma_n^2} \end{cases} \tag{4}$$

$$MSRCR_c\,(x,y) = \begin{cases} 0 & MSR_c\,(x,y) \le \min \\ \dfrac{(MSR_c\,(x,y) - \min)}{(\max - \min)} * 255 & \min < MSR_c\,(x,y) < \max \\ 255 & MSR_c\,(x,y) \ge \max \end{cases} \tag{5}$$

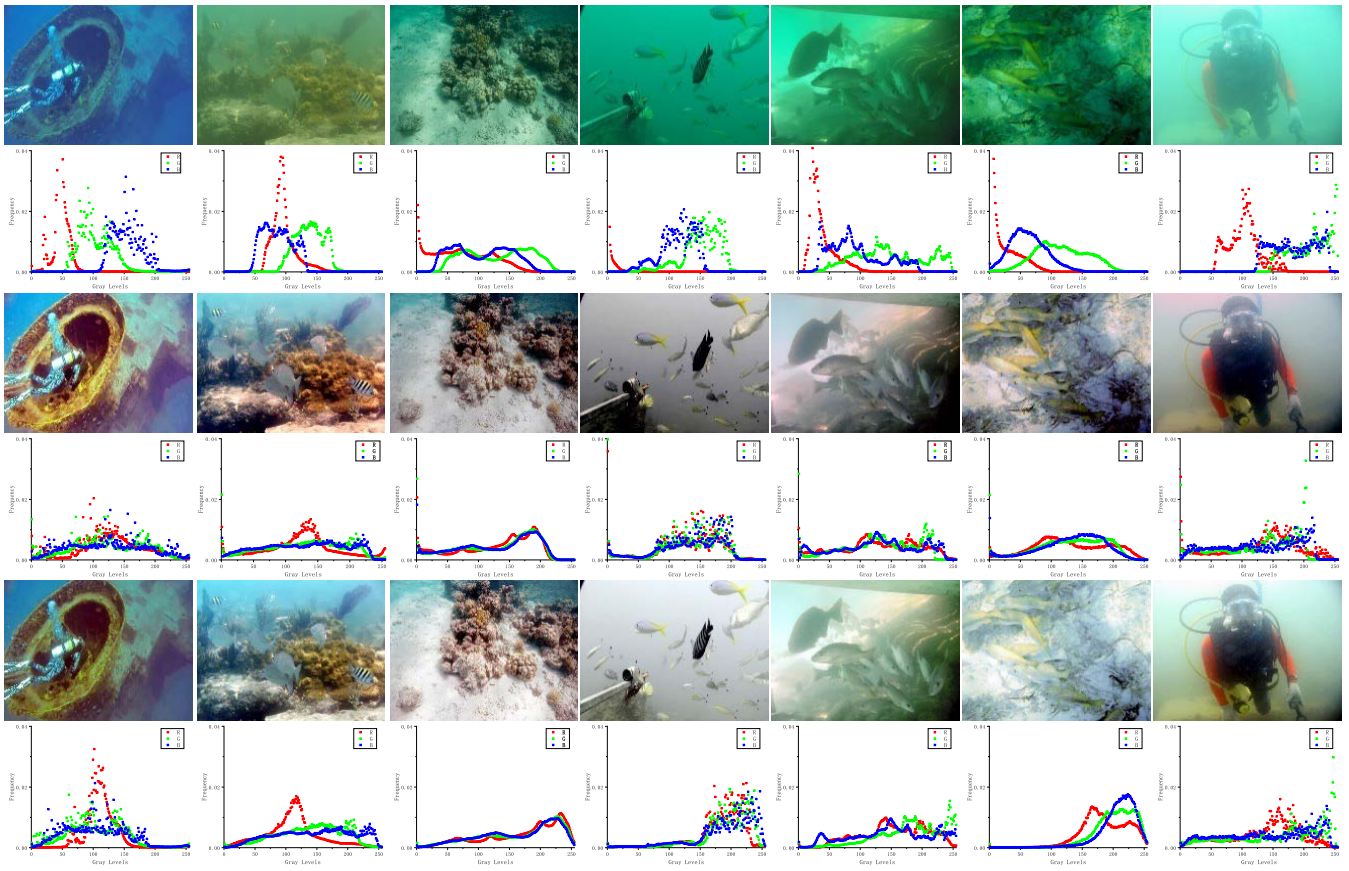

FIGURE 4. Comparison of different color correction methods: 1. The first row is original image; 2. The third row is color-corrected image of MSRCR; 3. The fifth row is color-corrected image of auto-levels-based MSR; 4. The remaining rows are tricolor histogram.

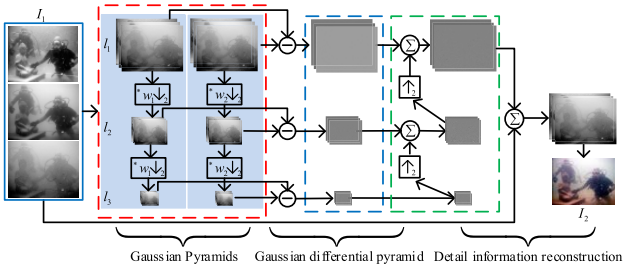

FIGURE 5. Flowchart of detail sharpening.

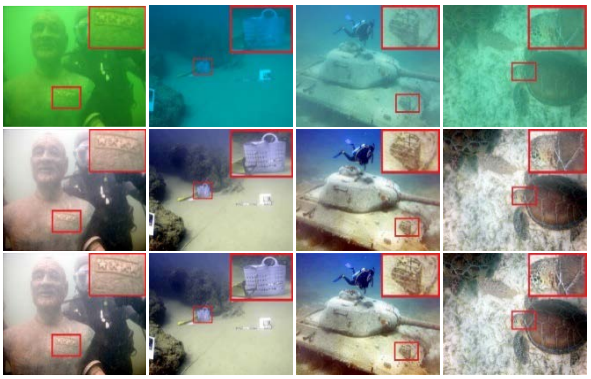

FIGURE 6. Comparison before and after sharpening details: 1. The first row is original image; 2. The second row is color-corrected images; 3. The third row is detail sharpened images.

and image I_1 are fused to obtain the sharpened image I_2 as follows:

$$I_2(i,j) = I_d(i,j) + I_1(i,j) \tag{9}$$

The second and third rows of Fig. 6 show that the more the area detail with higher contrast, and the more blurred the details of the area with lower contrast. The operation highlights the details better, but the effect is poor and limited color improvement for low-contrast areas. Therefore, we suggest further processing of the images using the CHALE method in the D section.

B. LOCAL CONTRAST ENHANCEMENT

Based on color correction and detail sharpening, the final enhanced image has richer color information and a more extensive dynamic range to improve the image further. Therefore, it is necessary to carry out pixel balance on the three-color channels of the image. AHE [58] is an improved method of traditional histogram equalization, but the method

has low robustness and high complexity. CLAHE [59] is an improved method of AHE, which limits the enhancement amplitude of local contrast by the height of CLAHE to suppress image noise and better preserve image details.

Based on CLAHE, the detailed steps of local contrast enhancement are as follows:

Step 1: The original image was divided into k non-overlapping sub-blocks of $M \times N$ size.

Step 2: Calculate the histogram of k subblocks, and the gray level of each histogram is r, the gray level is $NumGray$, then the histogram function corresponding to k subblocks is $T_{m,n}(r)$, $0 \leq r \leq NumGray - 1$.

Step 3: To determine the clip limit value, the pixel number in the sub-region is distributed to the average value of each gray level $AvgPixels$ can be expressed as follows:

$$AvgPixels = \frac{M \times N}{NumGray} \tag{10}$$

Limiting the number of pixels contained each grayscale level not exceeding the NClip of $AvgPixels$, thereby the actual clipping limit value CLimit is:

$$CLimit = AvgPixels \times \alpha \ (0 < \alpha \leq 1) \tag{11}$$

where α is clip coefficient, which represents the maximum percentage of pixels allowed for each gray level. The local contrast enhancement effect is not obvious when the clip value is too large, and the local contrast enhancement is oversaturated when the clip value is too small. The effect of local contrast enhancement is more ideal when the clip coefficient $\alpha = 5\%$ is determined by extensive experiments.

Step 4: Clipping the gray histogram of each subblock, and the number of clip pixels is reassigned to each grayscale of each histogram. Assuming that the total number of clipped pixels is AllClipPixels, the clipped pixel number of each gray level AvgClipPixels can be expressed as:

$$AvgClipPixels = \frac{AllClipPixels}{NumGray} \tag{12}$$

Then the redistribution process is expressed as:

$$\begin{cases} Num(i) = CLimit & CLimit < Num(i) \\ Num(i) = CLimit & CLimit \leq Num(i) + AvgClipPixels \\ Num(i) = Num(i) + & AvgClipPixels\ CLimit > Num(i) \end{cases} \tag{13}$$

where $Num(i)$ represents the number of pixels in the i^{th} grayscale in the original area. For the remaining pixels, a new histogram is obtained by looping Eq. (13) from the small grayscale level until the remaining pixels are 0.

Step 5: Each clipped histogram is enhanced by Rayleigh distribution and converted into cumulative probability. The expression of Rayleigh transformation can be expressed as:

$$Ray(i) = Ray_{\min} + \sqrt{2\alpha^2 \ln\left(\frac{1}{1 - P_{input}(i)}\right)} \tag{14}$$

FIGURE 7. Comparison before and after local contrast enhancement: 1. The first row is original image; 2. The second row is detail sharpened images; 3. The third row is contrast stretched images.

where $Ray_{\min}$ represents the lower limit of the pixel value, and α represents the scale parameter. Then the output probability of each intensity value can be defined as:

$$P(Ray(i)) = \frac{(Ray(i) - Ray_{\min})}{\alpha^2} \cdot \exp\left(-\frac{(Ray(i) - Ray_{\min})^2}{2\alpha^2}\right) \quad for\ Ray(i) \geq Ray_{\min} \tag{15}$$

When α value is large, it is easy to cause the image to be over-contrasted, while amplifying the noise and increasing the saturation value.

Step 6: To reduce the mutation effect, the output of the transformation function (15) is adjusted according to equation (16) by linear local contrast enhancement. Where the input values of transformation function $O(i)$, $O_{\max}$ and $O_{\min}$ are the values of the transformation function.

$$P_{out}(i) = \frac{O(i) - O_{\min}}{O_{\max} - O_{\min}} \tag{16}$$

Step 7: In order to remove the boundary artifacts, and the bilinear interpolation is performed for each pixel to obtain a new gray value. Suppose that the four sample points are (x_-, y_-), (x_+, y_-), (x_-, y_+), and (x_+, y_+), and the corresponding gray values are $G_{--}(i)$, $G_{+-}(i)$, $G_{-+}(i)$, and $G_{++}(i)$ respectively. The interpolation formula is defined as:

$$G(i) = a\left[bG_{--}(i) + (1-b)G_{+-}(i)\right] + (1-a)\left[bG_{-+}(i) + (1-b)G_{++}(i)\right] \tag{17}$$

where $a = (y - y_-)/(y_+ - y_-)$ and $b = (x - x_-)/(x_+ - x_-)$.

Comparing the second and third rows of Fig. 7, the stretched underwater image has high contrast, rich color, and the dark area of the sea floor is better enhanced due to the effective stretching of contrast.

V. EXPERIMENTAL RESULTS AND ANALYSIS

We first carried out a comprehensive evaluation of color accuracy. Then, we qualitatively and quantitatively compare existing methods based on various underwater image data captured from complex scenes. Finally, we provide an application on key feature point matching.

FIGURE 8. Comparison the color accuracy of different sharpening methods. From left to right: 1. Original image, 2. EUIV [47], 3. UDER [20], 4. MILHD [60], 5. GDCP [61], 6. UICR [62], 7. Our results.

A. COLOR ACCURACY TEST

To verify the accuracy of our method for color restoration, we chose ColorChecker Chart 24 as a reference for color accuracy. We compared the following methods: EUIV [47], UDER [20], MILHD [60], GDCP [61], and UICR [62]. The comparison results are shown in Fig. 8.

As shown in Fig. 8, in terms of global color restoration, UDER [20] and GDCP [61] can't completely remove the color cast. EUIV [47], MILHD [60] and UICR [62] obtained good results, but MILHD [60] and UICR [62] presented reddish and dark appearance respectively. However, our method has better visual effects and higher color accuracy. In terms of local color restoration, the color accuracy of UDER [20], GDCP [61], and UICR [62] are not ideal. EUIV [47] and MILHD [60] show better results, but our method has high robustness for different camera-captured underwater images regarding color fidelity.

B. UNDERWATER ENHANCING EVALUATION

We first evaluate our method using the dataset of UICR [62]. Which mainly includes the color charts and the 3D structure of the scene [62], [63]. The configuration details of this underwater image and acquisition camera set are in [62]. We compared the following methods: UDER [20], MILHD [60], IBLA [6], Tstep [64], GDCP [61], and UICR [62]. The comparison results are shown in Fig. 9. Table 1 and Table 2 provide the five-evaluation metrics the five metrics are information entropy (IE) [55], average gradient (AG) [55], patch-based contrast quality index (PCQI) [65], underwater image colorfulness measure (UIQM) [66], and underwater color image quality evaluation (UCIQE) [67]. Where IE, AG, and PCQI are normal metrics for natural image enhancement methods, UIQM and UCIQE are special metrics for underwater image enhancement methods. IE is employed to evaluate the color information of the image. AG is employed to evaluate the clarity of the image. PCQI is used for the human eye's perception of image contrast. UIQM evaluates the quality of underwater images by the colorfulness, sharpness, and contrast of underwater images. UNIQUE evaluates the quality of underwater images by the linear combination of chroma, saturation, and contrast of underwater images.

Fig. 9 shows that the methods of IBLA [6] and GDCP [61] are not ideal for color correction and contrast enhancement of underwater scenes. UDER [20] and MILHD [60] are better than IBLA [6] and GDCP [61] in restoring the contrast of the scene. However, UDER [20] and MILHD [60] still have significant color bias. For instance, the restoration results of

TABLE 1. Quantitative results based on IE, AG and UIQM metrics for each method in Fig. 9.

	UDER			MILHD			IBLA			Tstep			GDCP			UICR			Our method		
	IE	AG	UIQM	IE	AG	UIQM	IE	AG	UIQM	IE	AG	UIQM	IE	AG	UIQM	IE	AG	UIQM	IE	AG	UIQM
R3008	6.87	2.87	0.97	6.94	2.95	1.01	7.02	1.84	1.02	7.48	2.94	0.99	7.14	2.29	1.05	7.38	2.65	1.00	7.86	5.42	1.22
R3204	6.75	1.37	0.82	7.22	1.61	0.93	7.10	1.33	1.00	7.57	2.07	0.94	6.95	1.34	0.95	7.17	1.37	0.89	7.83	2.97	1.14
R4485	5.89	1.96	0.91	5.99	5.33	1.00	6.21	1.57	1.09	6.83	1.96	0.94	6.38	2.14	1.05	6.70	3.31	1.18	7.85	6.67	1.2
R4491	5.71	1.96	0.81	6.17	9.25	1.10	6.42	2.11	1.14	7.17	2.99	0.95	6.25	2.52	1.06	5.92	7.49	1.13	7.88	8.13	1.31
R5450	5.38	0.66	0.83	5.66	3.64	0.93	5.71	0.60	1.04	6.28	0.72	0.89	5.68	0.67	0.91	5.69	1.56	1.05	7.25	1.75	1.03
R5469	5.93	1.09	0.90	6.12	4.51	0.95	6.28	0.93	1.07	6.75	1.09	0.91	6.11	1.20	0.96	5.91	2.11	1.00	7.43	2.84	1.12
R5478	5.81	0.92	0.89	5.88	4.58	0.94	6.09	0.76	1.05	6.72	0.96	0.91	5.84	0.96	0.94	5.02	1.85	0.96	7.70	2.71	1.07
Average	6.05	1.55	0.88	6.28	**4.55**	0.98	6.40	1.31	1.06	6.97	1.82	0.93	6.34	1.59	0.99	6.26	2.91	1.03	**7.69**	**4.36**	**1.16**

TABLE 2. Quantitative results based on IE, PCQI, UIQM and UCIQE metrics for each method in Fig. 10.

	EUIV				UDER				IBLA				Tstep				GDCP				UICR				Our method			
	IE	PCQI	UIQM	UCIQE	IE	PCQI	UIQM	UCIQE	IE	PCQI	UIQM	UCIQE	IE	PCQI	UIQM	UCIQE	IE	PCQI	UIQM	UCIQE	IE	PCQI	UIQM	UCIQE	IE	PCQI	UIQM	UCIQE
Diver1	7.94	1.05	2.16	0.373	6.49	0.78	0.032	0.576	7.65	0.99	0.35	0.3733	7.60	0.92	3.46	0.5865	7.60	1.01	0.45	0.5117	7.51	0.79	2.44	0.6209	7.75	1.14	3.26	0.5962
Diver2	7.74	1.04	5.31	0.496	5.63	0.71	1.02	0.584	7.29	1.12	0.84	0.4963	7.16	1.07	2.73	0.5713	7.55	0.97	-0.306	0.4897	6.70	0.89	2.79	0.6051	7.84	1.23	3.10	0.663
Diver3	7.83	1.29	4.51	0.435	7.21	1.02	3.03	0.560	7.66	1.15	2.95	0.4355	7.47	1.19	4.54	0.5457	7.70	1.08	1.09	0.4807	7.62	1.06	4.33	0.6318	7.93	1.32	4.96	0.6095
Diver4	7.85	1.23	3.67	0.430	5.71	0.65	2.04	0.533	7.56	1.08	1.82	0.4309	7.42	1.09	4.67	0.5657	7.63	1.09	4.64	0.6367	7.28	0.73	3.49	0.6392	7.87	1.29	4.46	0.6046
Fish1	7.88	1.23	3.10	0.290	5.36	0.95	1.33	0.472	6.52	1.14	2.42	0.2909	6.38	0.94	2.38	0.375	5.78	1.23	1.65	0.4075	7.10	1.22	2.04	0.6671	7.92	1.36	4.68	0.676
Fish2	7.77	1.15	4.37	0.299	6.34	0.98	1.05	0.577	7.25	1.12	-1.235	0.2992	7.10	0.99	1.38	0.4357	6.99	1.14	-2.86	0.3613	7.57	1.10	1.92	0.5887	7.95	1.34	4.46	0.6046
Coral reef1	7.95	1.19	4.33	0.495	6.90	0.89	3.96	0.543	7.79	1.05	24.37	0.4959	7.79	1.13	4.83	0.5883	7.73	1.11	22.42	0.6526	7.40	0.76	4.08	0.6157	7.94	1.21	4.99	0.609
Average	7.85	1.17	3.92	0.403	6.23	0.85	1.78	0.549	7.39	1.09	**4.50**	0.4031	7.27	1.05	3.42	0.5240	7.28	1.09	3.87	0.5057	7.31	0.94	3.01	0.6240	**7.89**	**1.27**	4.27	**0.6232**

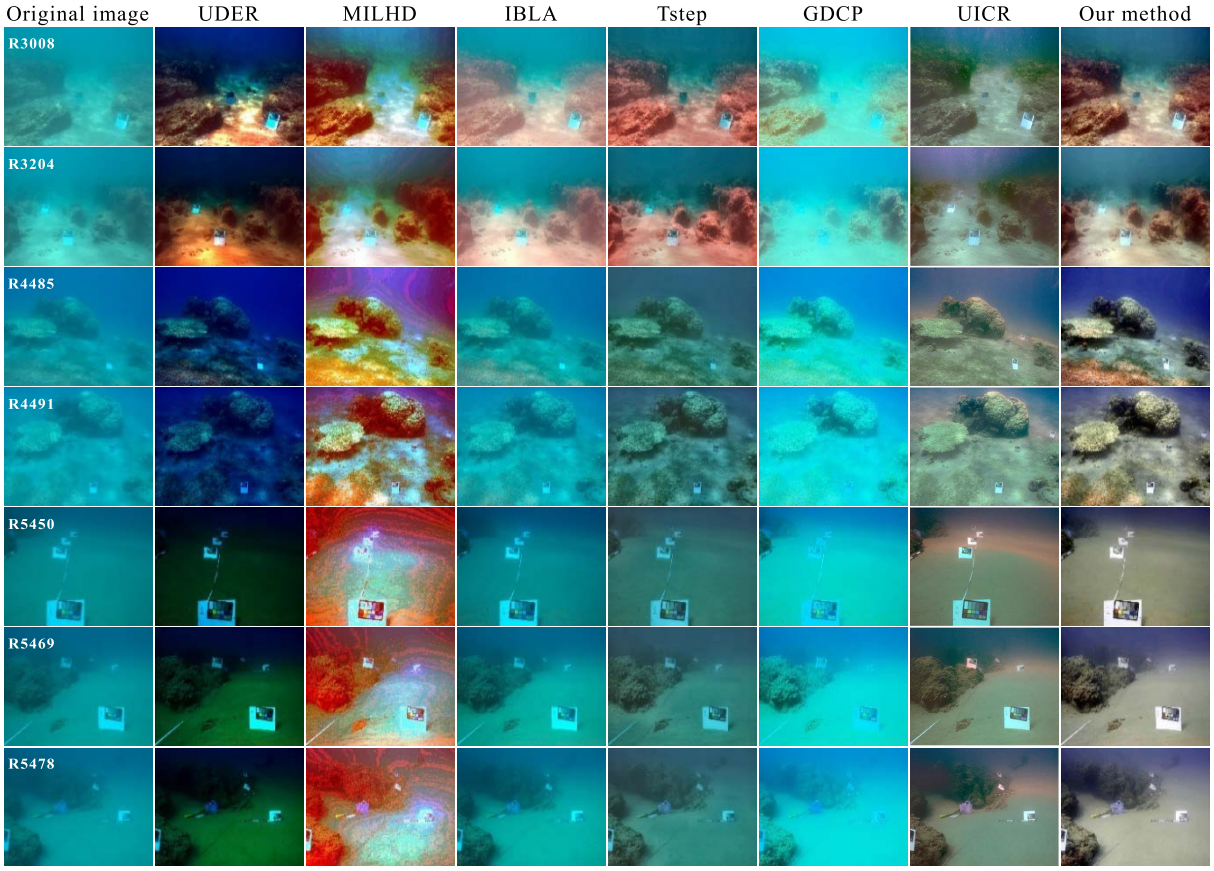

FIGURE 9. Comparison the results of different methods. From left to right: 1. Original image, 2. UDER [20], 3. MILHD [60], 4. IBLA [6], 5. Tstep [64], 6. GDCP [61], 7. UICR [62], 8. Our results. The result of the correspond to these images is shown in Table 1.

R3008 and R3204 obtained by UDER [20] are significantly reddish in appearance, while the restoration results of other images are slightly blue and dark. This set of underwater images is enhanced by MILHD [60] with an obvious reddish appearance. Tstep [64] has higher robustness in restoring the scene's contrast, but there is some color bias, such as the enhanced images of the R3008 and R3204 with a reddish appearance. UICR [62] has higher robustness in restoring

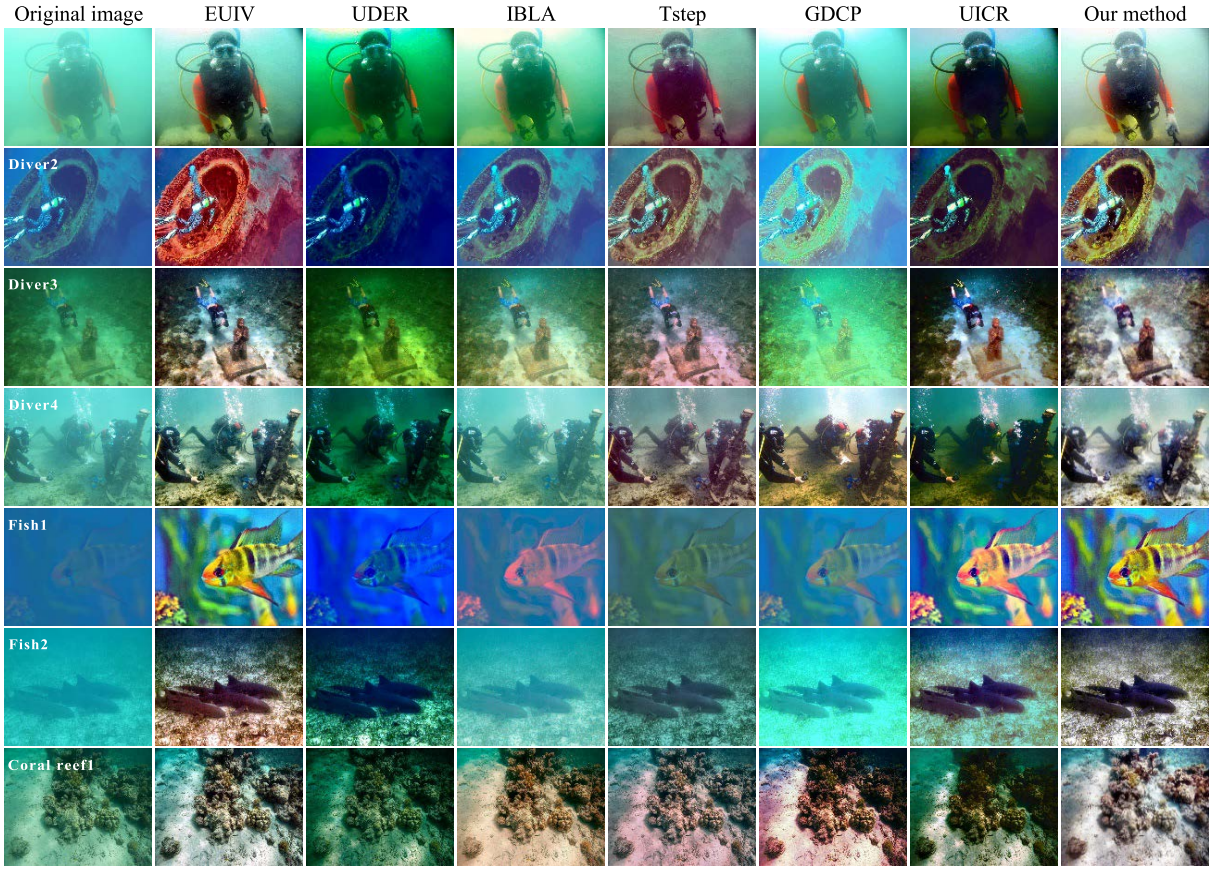

FIGURE 10. Comparison the results of different methods. From left to right: 1. Original image, 2. EUIV [47], 3. UDER [20], 4. IBLA [6], 5. Tstep [64], 6. GDCP [61], 7. UICR [62], 8. Our results. The result of the correspond to these images is shown in Table 2.

scene contrast and color, but the recovered image with the problem of blurring the details. Our methods are superior to comparison methods in color correction, contrast, and detail enhancement and have similar or usually higher values of IE, AG, and UIQM metrics in Table 1.

As shown in Fig. 10, as can be observed that UDER [20], IBLA [6], and GDCP [61] didn't perform well. EUIV [47] and Tstep [64] have higher robustness in restoring the contrast of the scene, but they also have some color bias. For example, the enhanced image of Diver2 with reddish was obtained by EUIV [47], and the restored images of Diver4 and Coral reef1 with reddish were obtained by Tstep [64]. In spite of UICR [62] performing well for underwater scenes, details of the restored images are lost. For instance, the restored images of Fish2 with overexposure and detail loss were obtained by UICR [62]. As shown in Table 2, our method is significantly better than other methods.

As shown in Fig. 10, as can be observed that UDER [20], IBLA [6], and GDCP [61] didn't perform well. EUIV [47] and Tstep [64] have higher robustness in restoring the contrast of the scene, but they also have some color bias. For example, the enhanced image of Diver2 with reddish was obtained by EUIV [47], and the restored images of Diver4 and Coral reef1 with reddish were obtained by Tstep [64]. Despite UICR [62] performing well for underwater scenes, details of the restored images are lost. For instance, the restored images of Fish2 with overexposure and detail loss were obtained by UICR [62]. As shown in Table 2, our method is significantly better than other methods.

TABLE 3. Running time with IBLA [6], UDER [20], GDCP [61], UICR [62], MILHD [60], Tstep [64], EUIV [47], and our method.

Image Resolution	IBLA	UDER	GDCP	UICR	MILHD	Tstep	EUIV	Our method
400 × 300	28.35	14.78	2.25	35.65	0.95	0.32	0.49	0.43
550 × 412	56.92	30.32	3.9	90.1	1.69	0.49	0.89	0.70
853 × 600	129.01	70.03	8.95	121.03	4.01	1.01	1.91	1.60
907 × 757	158.98	84.52	9.23	23.74	4.75	1.21	2.31	1.92
1024 × 738	183.85	96.98	13.4	249.92	5.51	1.28	2.67	2.35
1920 × 1080	489.52	259.44	24.62	251.78	13.01	2.91	6.24	4.92
2208 × 1474	789.98	414.76	51.82	105.19	21.96	4.59	9.55	8.78

To compare the running time, on the basis of the same hardware configuration, system, and Matlab R2019b, the average time of each method running ten times is shown in Table 3. It can be seen that our method outperforms other comparison methods. The advantage becomes more pronounced with an increase in image resolution. UDER [20], IBLA [6], GDCP [61], and UICR [62] are based on the methods of solving complex physical models and therefore run longer. MILHD [60] increased the complexity of the method. EUIV [47] is slightly more complicated than our

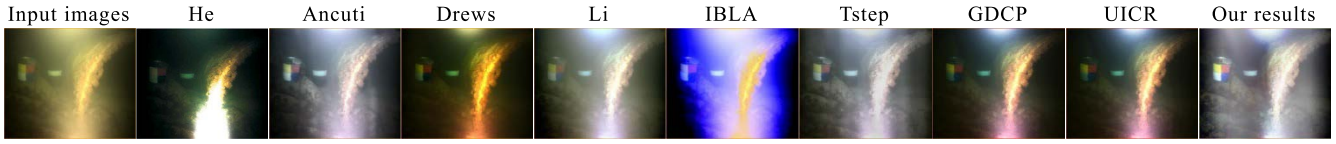

FIGURE 11. Comparison results in extreme scenes with the nonuniform illumination condition. from left to right: 1. DCP [18], 2. EUIV [47], 3. UDER [20],4. IBLA [6], 5. Tstep [64], 6. GDCP [61],7. UICR [62], 8. Our results.

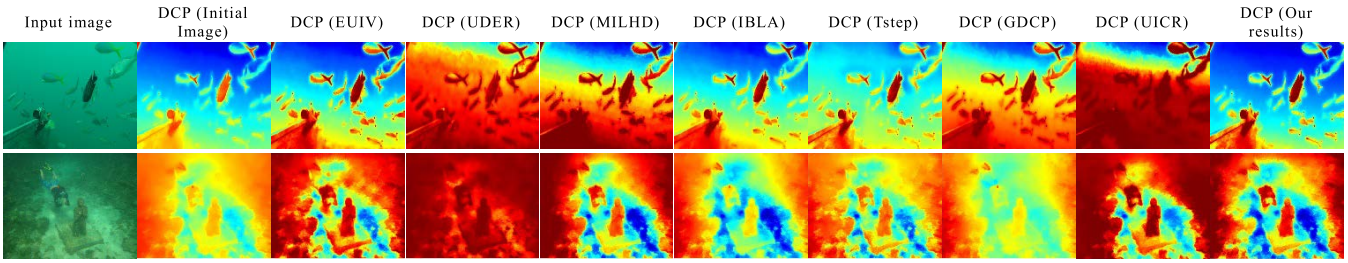

FIGURE 12. Comparison results on underwater transmission estimation. from left to right: 1. EUIV [47], 2. UDER [20], 3. MILHD [60], 4. IBLA [6], 5. Tstep [64], 6. GDCP [61], 7. UICR [62], Our results.

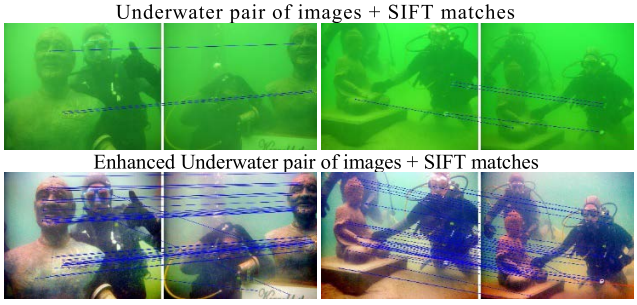

FIGURE 13. Applying standard SIFT significantly improves the accuracy of point matching on our enhanced image (bottom) compared to the original underwater image (top).

method because of the use of too many fusion images and weight maps. Tstep [64] doesn't require too many complex operations and therefore is superior to our method. The running time of IBLA [6], UDER [20], GDCP [61], UICR [62], and MILHD [60] is significantly increasing with the rapid increase in image resolution, while Tstep [64], EUIV [43] and our method are slowly growing.

Besides, Fig. 11 further considers that captured underwater images usually appear yellowish and have low contrast. For such images, we need to perform color compensation, which can effectively correct the image's color. It can be seen from Fig. 11 that our method outperforms the other methods. Fig. 12 shows that the proposed method has significantly improved the estimation of transmission maps based on DCP [18]. It can be seen that UDER [20], Tstep [64], and GDCP [61] estimate that the effectiveness of the transmission map is poor. In contrast, EUIV [47], IBLA [6], and UICR [62] are superior to them in the estimation of transmission maps. Furthermore, MILHD [60] method has a good transmittance estimation performance, but some details are lost. However, our method significantly improves transmission map estimation and highlights the details.

C. APPLICATION

The purpose of enhancing the underwater image is to benefit autonomous underwater navigation [68], underwater target tracking [69], and key feature point matching [48]. To verify the application effect of our method after image enhancement using the key feature point matching as an example.

Fig. 13 shows feature matching results using SIFT on the original and enhanced images. It is not difficult to see that more feature matching points can be obtained under the same threshold condition by using our method to enhance the image.

VI. CONCLUSION

We propose an underwater image enhancement method, which mainly includes four parts: color compensation, color correction, detail sharpening, and contrast enhancement. Our proposed method realizes the color compensation from multi-channel to color correction. It solves the detail blurring and low contrast by the detail sharpening of the Gaussian differential pyramid and the local contrast enhancement of CLAHE. Experimental results show that our method improves contrast, detail information, and color correction by multi-scale Retinex (MSR) based on auto-levels. In particular, our method maintains the advantages of both qualitative and quantitative metrics and has fast and highly efficient performance.

REFERENCES

[1] W. Zhang, P. Zhuang, H.-H. Sun, G. Li, S. Kwong, and C. Li, "Underwater image enhancement via minimal color loss and locally adaptive contrast enhancement," *IEEE Trans. Image Process.*, vol. 31, pp. 3997–4010, 2022.

[2] C. Li, S. Anwar, J. Hou, R. Cong, C. Guo, and W. Ren, "Underwater image enhancement via medium transmission-guided multi-color space embedding," *IEEE Trans. Image Process.*, vol. 30, pp. 4985–5000, 2021.

[3] Z. Jiang, Z. Li, S. Yang, X. Fan, and R. Liu, "Target oriented perceptual adversarial fusion network for underwater image enhancement," *IEEE Trans. Circuits Syst. Video Technol.*, vol. 14, no. 8, pp. 1–15, Aug. 2021.

[4] W. Zhang, Y. Wang, and C. Li, "Underwater image enhancement by attenuated color channel correction and detail preserved contrast enhancement," *IEEE J. Ocean. Eng.*, vol. 47, no. 3, pp. 1–18, Mar. 2022.
[5] P. Zhuang, J. Wu, F. Porikli, and C. Li, "Underwater image enhancement with hyper-Laplacian reflectance priors," *IEEE Trans. Image Process.*, vol. 31, pp. 5442–5455, 2022.
[6] Y.-T. Peng and P. C. Cosman, "Underwater image restoration based on image blurriness and light absorption," *IEEE Trans. Image Process.*, vol. 26, no. 4, pp. 1579–1594, Apr. 2017.
[7] A. S. A. Ghani and N. A. M. Isa, "Underwater image quality enhancement through integrated color model with Rayleigh distribution," *Appl. Soft Comput.*, vol. 27, pp. 219–230, Feb. 2015.
[8] X. Zhao, T. Jin, and S. Qu, "Deriving inherent optical properties from background color and underwater image enhancement," *Ocean Eng.*, vol. 94, pp. 163–172, Jan. 2015.
[9] C. Li, J. Guo, and C. Guo, "Emerging from water: Underwater image color correction based on weakly supervised color transfer," *IEEE Signal Process. Lett.*, vol. 25, no. 3, pp. 323–327, Mar. 2018.
[10] M. Levoy, B. Chen, V. Vaish, M. Horowitz, I. McDowall, and M. Bolas, "Synthetic aperture confocal imaging," *ACM Trans. Graph.*, vol. 23, no. 3, pp. 825–834, Aug. 2004.
[11] T. Treibitz and Y. Y. Schechner, "Turbid scene enhancement using multi-directional illumination fusion," *IEEE Trans. Image Process.*, vol. 21, no. 11, pp. 4662–4667, Jul. 2012.
[12] B. Ouyang, F. Dalgleish, A. Vuorenkoski, W. Britton, B. Ramos, and B. Metzger, "Visualization and image enhancement for multistatic underwater laser line scan system using image-based rendering," *IEEE J. Ocean. Eng.*, vol. 38, no. 3, pp. 566–580, Jul. 2013.
[13] S. G. Narasimhan and S. K. Nayar, "Contrast restoration of weather degraded images," *IEEE Trans. Pattern Anal. Mach. Learn.*, vol. 25, no. 6, pp. 713–724, Jun. 2003.
[14] Y. Y. Schechner and Y. Averbuch, "Regularized image recovery in scattering media," *IEEE Trans. Pattern Anal. Mach. Intell.*, vol. 29, no. 9, pp. 1655–1660, Sep. 2007.
[15] T. Treibitz and Y. Y. Schechner, "Active polarization descattering," *IEEE Trans. Pattern Anal. Mach. Intell.*, vol. 31, no. 3, pp. 385–399, Mar. 2009.
[16] J. Kopf, B. Neubert, B. Chen, M. Cohen, D. Cohen-Or, O. Deussen, M. Uyttendaele, and D. Lischinski, "Deep photo: Model-based photograph enhancement and viewing," *ACM Trans. Graph.*, vol. 27, no. 5, pp. 1–10, Dec. 2008.
[17] Y. Tian, B. Liu, X. Su, L. Wang, and K. Li, "Underwater imaging based on LF and polarization," *IEEE Photon. J.*, vol. 11, no. 1, pp. 1–9, Feb. 2019.
[18] K. He, J. Sun, and X. Tang, "Single image haze removal using dark channel prior," *IEEE Trans. Pattern Anal. Mach. Intell.*, vol. 33, no. 12, pp. 2341–2353, Dec. 2011.
[19] P. Drews, E. do Nascimento, F. Moraes, S. Botelho, and M. Campos, "Transmission estimation in underwater single images," in *Proc. IEEE Int. Conf. Comput. Vis. Workshops*, Dec. 2013, pp. 825–830.
[20] P. L. J. Drews, E. R. Nascimento, S. S. C. Botelho, and M. F. M. Campos, "Underwater depth estimation and image restoration based on single images," *IEEE Comput. Graph. Appl.*, vol. 36, no. 2, pp. 24–35, Mar. 2016.
[21] M. Zhang and J. Peng, "Underwater image restoration based on a new underwater image formation model," *IEEE Access*, vol. 6, pp. 58634–58644, 2018.
[22] Y. Liu, S. Rong, X. Cao, T. Li, and B. He, "Underwater single image dehazing using the color space dimensionality reduction prior," *IEEE Access*, vol. 8, pp. 91116–91128, 2020.
[23] Y. Fang, W. Lin, B.-S. Lee, C.-T. Lau, Z. Chen, and C.-W. Lin, "Bottom-up saliency detection model based on human visual sensitivity and amplitude spectrum," *IEEE Trans. Multimedia*, vol. 14, no. 1, pp. 187–198, Sep. 2012.
[24] M.-J. Seow and V. K. Asari, "Ratio rule and homomorphic filter for enhancement of digital colour image," *Neurocomputing*, vol. 69, nos. 7–9, pp. 954–958, Mar. 2006.
[25] S.-B. Gao, M. Zhang, Q. Zhao, X.-S. Zhang, and Y.-J. Li, "Underwater image enhancement using adaptive retinal mechanisms," *IEEE Trans. Image Process.*, vol. 28, no. 11, pp. 5580–5595, Nov. 2019.
[26] S. Wang, K. Gu, S. Ma, W. Lin, X. Liu, and W. Gao, "Guided image contrast enhancement based on retrieved images in cloud," *IEEE Trans. Multimedia*, vol. 18, no. 2, pp. 219–232, Feb. 2015.
[27] H. Xu, G. Zhai, X. Wu, and X. Yang, "Generalized equalization model for image enhancement," *IEEE Trans. Multimedia*, vol. 16, no. 1, pp. 68–82, Jan. 2013.
[28] A. S. A. Ghani and N. A. M. Isa, "Enhancement of low quality underwater image through integrated global and local contrast correction," *Appl. Soft Comput.*, vol. 37, pp. 332–344, Dec. 2015.
[29] R. Hummel, "Image enhancement by histogram transformation," *Comput. Graph. Image Process.*, vol. 6, no. 2, pp. 184–195, Apr. 1977.
[30] S. M. Pizer, E. P. Amburn, J. D. Austin, R. Cromartie, A. Geselowitz, T. Greer, B. ter Haar Romeny, J. B. Zimmerman, and K. Zuiderveld, "Adaptive histogram equalization and its variations," *Comput. Vis., Graph., Image Process.*, vol. 39, no. 3, pp. 355–368, Sep. 1987.
[31] M. S. Hitam, W. N. J. H. W. Yussof, E. A. Awalludin, and Z. Bachok, "Mixture contrast limited adaptive histogram equalization for underwater image enhancement," in *Proc. Int. Conf. Comput. Appl. Technol. (ICCAT)*, Jan. 2013, pp. 1–5.
[32] Y.-C. Liu, W.-H. Chan, and Y.-Q. Chen, "Automatic white balance for digital still camera," *IEEE Trans. Consum. Electron.*, vol. 41, no. 3, pp. 460–466, Aug. 1995.
[33] G. Buchsbaum, "A spatial processor model for object colour perception," *J. Franklin Inst.*, vol. 310, no. 1, pp. 1–26, Jul. 1980.
[34] J. van de Weijer, T. Gevers, and A. Gijsenij, "Edge-based color constancy," *IEEE Trans. Image Process.*, vol. 16, no. 9, pp. 2207–2214, Sep. 2007.
[35] A. Gijsenij, T. Gevers, and J. van de Weijer, "Improving color constancy by photometric edge weighting," *IEEE Trans. Pattern Anal. Mach. Intell.*, vol. 34, no. 5, pp. 918–929, May 2011.
[36] Y. Gao, H.-M. Hu, B. Li, and Q. Guo, "Naturalness preserved nonuniform illumination estimation for image enhancement based on Retinex," *IEEE Trans. Multimedia*, vol. 20, no. 2, pp. 335–344, Feb. 2017.
[37] K. R. Joshi and R. S. Kamathe, "Quantification of retinex in enhancement of weather degraded images," in *Proc. Int. Conf. Audio, Lang. Image Process.*, Jul. 2008, pp. 1229–1233.
[38] X. Fu, P. Zhuang, Y. Huang, Y. Liao, X.-P. Zhang, and X. Ding, "A retinex-based enhancing approach for single underwater image," in *Proc. IEEE Int. Conf. Image Process. (ICIP)*, Oct. 2014, pp. 4572–4576.
[39] S. M. Alex and M. H. Supriya, "Underwater image enhancement using single scale retinex on a reconfigurable hardware," in *Proc. Int. Symp. Ocean Electron. (SYMPOL)*, Nov. 2015, pp. 1–5.
[40] J. Perez, A. C. Attanasio, N. Nechyporenko, and P. J. Sanz, "A deep learning approach for underwater image enhancement," in *Proc. Int. Work-Conf. Interplay Between Natural Artif. Comput.* Cham, Switzerland: Springer, 2017, pp. 183–192.
[41] W. Zhang, L. Dong, and W. Xu, "Retinex-inspired color correction and detail preserved fusion for underwater image enhancement," *Comput. Electron. Agricult.*, vol. 192, Jan. 2022, Art. no. 106585.
[42] X. Zong, Z. Chen, and D. Wang, "Local-CycleGAN: A general end-to-end network for visual enhancement in complex deep-water environment," *Appl. Intell.*, vol. 51, no. 4, pp. 1947–1958, Oct. 2021.
[43] W. Zhang, L. Dong, T. Zhang, and W. Xu, "Enhancing underwater image via color correction and bi-interval contrast enhancement," *Signal Process., Image Commun.*, vol. 90, Jan. 2021, Art. no. 116030.
[44] S. Sun, H. Wang, H. Zhang, M. Li, M. Xiang, C. Luo, and P. Ren, "Underwater image enhancement with reinforcement learning," *IEEE J. Ocean. Eng.*, early access, Apr. 7, 2022, doi: 10.1109/JOE.2022.3152519.
[45] R. Liu, Z. Jiang, S. Yang, and X. Fan, "Twin adversarial contrastive learning for underwater image enhancement and beyond," *IEEE Trans. Image Process.*, vol. 31, pp. 4922–4936, 2022.
[46] J. Wang, P. Li, J. Deng, Y. Du, J. Zhuang, P. Liang, and P. Liu, "CA-GAN: Class-condition attention GAN for underwater image enhancement," *IEEE Access*, vol. 8, pp. 130719–130728, 2020.
[47] C. Ancuti, C. O. Ancuti, T. Haber, and P. Bekaert, "Enhancing underwater images and videos by fusion," in *Proc. IEEE Conf. Comput. Vis. Pattern Recognit.*, Jun. 2012, pp. 81–88.
[48] C. O. Ancuti, C. Ancuti, C. De Vleeschouwer, and P. Bekaert, "Color balance and fusion for underwater image enhancement," *IEEE Trans. Image Process.*, vol. 27, no. 1, pp. 379–393, Jan. 2018.
[49] R. Sethi and S. Indu, "Fusion of underwater image enhancement and restoration," *Int. J. Pattern Recognit. Artif. Intell.*, vol. 34, no. 3, Mar. 2020, Art. no. 2054007.
[50] X. Liu, Z. Gao, and B. M. Chen, "MLFcGAN: Multilevel feature fusion-based conditional GAN for underwater image color correction," *IEEE Geosci. Remote Sens. Lett.*, vol. 17, no. 9, pp. 1488–1492, Sep. 2020.
[51] J. Y. Chiang and Y.-C. Chen, "Underwater image enhancement by wavelength compensation and dehazing," *IEEE Trans. Image Process.*, vol. 21, no. 4, pp. 1756–1769, Apr. 2012.

[52] S. Negahdaripour and A. Sarafraz, "Improved stereo matching in scattering media by incorporating a backscatter cue," *IEEE Trans. Image Process.*, vol. 23, no. 12, pp. 5743–5755, Dec. 2014.
[53] S. Zhang, T. Wang, J. Dong, and H. Yu, "Underwater image enhancement via extended multi-scale Retinex," *Neurocomputing*, vol. 245, Jul. 2017, pp. 1–9.
[54] D. J. Jobson, Z.-U. Rahman, and G. A. Woodell, "A multiscale Retinex for bridging the gap between color images and the human observation of scenes," *IEEE Trans. Image Process.*, vol. 6, no. 7, pp. 965–976, Jul. 1997.
[55] W. Zhang, L. Dong, X. Pan, J. Zhou, L. Qin, and W. Xu, "Single image defogging based on multi-channel convolutional MSRCR," *IEEE Access*, vol. 7, pp. 72492–72504, 2019.
[56] C. O. Ancuti and C. Ancuti, "Single image dehazing by multi-scale fusion," *IEEE Trans. Image Process.*, vol. 22, no. 8, pp. 3271–3282, Aug. 2013.
[57] L. Zhang, Y. Gao, Y. Xia, Q. Dai, and X. Li, "A fine-grained image categorization system by cellet-encoded spatial pyramid modeling," *IEEE Trans. Ind. Electron.*, vol. 62, no. 1, pp. 564–571, Jan. 2015.
[58] X. Sun, P. L. Rosin, R. R. Martin, and F. C. Langbein, "Bas-relief generation using adaptive histogram equalization," *IEEE Trans. Vis. Comput. Graphics*, vol. 15, no. 4, pp. 642–653, Aug. 2009.
[59] S. K. Wajid, A. Hussain, and K. Huang, "Three-dimensional local energy-based shape histogram (3D-LESH): A novel feature extraction technique," *Expert Syst. Appl.*, vol. 112, pp. 388–400, Dec. 2018.
[60] C.-Y. Li, J.-C. Guo, R.-M. Cong, Y.-W. Pang, and B. Wang, "Underwater image enhancement by dehazing with minimum information loss and histogram distribution prior," *IEEE Trans. Image Process.*, vol. 25, no. 12, pp. 5664–5677, Dec. 2016.
[61] Y.-T. Peng, K. Cao, and P. C. Cosman, "Generalization of the dark channel prior for single image restoration," *IEEE Trans. Image Process.*, vol. 27, no. 6, pp. 2856–2868, Jun. 2018.
[62] D. Berman, D. Levy, S. Avidan, and T. Treibitz, "Underwater single image color restoration using haze-lines and a new quantitative dataset," *IEEE Trans. Pattern Anal. Mach. Intell.*, vol. 43, no. 8, pp. 2822–2837, Aug. 2021.
[63] D. Berman, T. Treibitz, and S. Avidan, "Diving into haze-lines: Color restoration of underwater images," in *Proc. Brit. Mach. Vis. Conf. (BMVC)*, vol. 1, no. 2, 2017, pp. 1–12.
[64] X. Fu, Z. Fan, M. Ling, Y. Huang, and X. Ding, "Two-step approach for single underwater image enhancement," in *Proc. Int. Symp. Intell. Signal Process. Commun. Syst. (ISPACS)*, Nov. 2017, pp. 789–794.
[65] S. Wang, K. Ma, H. Yeganeh, Z. Wang, and W. Lin, "A patch-structure representation method for quality assessment of contrast changed images," *IEEE Signal Process. Lett.*, vol. 22, no. 12, pp. 2387–2390, Dec. 2015.
[66] K. Panetta, C. Gao, and S. Agaian, "Human-visual-system-inspired underwater image quality measures," *IEEE J. Ocean. Eng.*, vol. 41, no. 3, pp. 541–551, Jul. 2016.
[67] M. Yang and A. Sowmya, "An underwater color image quality evaluation metric," *IEEE Trans. Image Process.*, vol. 24, no. 12, pp. 6062–6071, Dec. 2015.
[68] J. Kim, H. Joe, S. C. Yu, J. S. Lee, and M. Kim, "Time-delay controller design for position control of autonomous underwater vehicle under disturbances," *IEEE Trans. Ind. Electron.*, vol. 63, no. 2, pp. 1052–1061, Feb. 2016.
[69] A.-A. Saucan, T. Chonavel, C. Sintes, and J.-M. Le Caillec, "CPHD-DOA tracking of multiple extended sonar targets in impulsive environments," *IEEE Trans. Signal Process.*, vol. 64, no. 5, pp. 1147–1160, Mar. 2016.

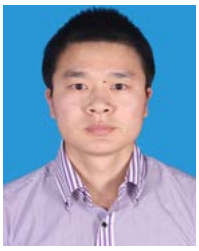

SONGLIN JIN received the M.S. degree in computer application technology from Central China Normal University, in 2010. Currently, he is a Lecturer with the Henan Institute of Science and Technology. His research interests include machine learning and hyperspectral image processing.

PEIXIN QU received the M.S. degree in physical electronics from Belarusian State University, in 2007. Currently, he is an Associate Professor with the Henan Institute of Science and Technology. His research interests include the areas of machine learning and wireless sensor networks.

YING ZHENG received the M.S. degree in computer software and theory from Henan Normal University, in 2013. Currently, she is a Lecturer with the Henan Institute of Science and Technology. Her research interests include machine learning, deep learning applications, and agricultural informatization.

WENYI ZHAO is currently pursuing the Ph.D. degree with the School of Artificial Intelligence, Beijing University of Posts and Telecommunications, Beijing, China. His research interests include machine learning, deep learning, and machine vision.

WEIDONG ZHANG received the Ph.D. degree in information and communication engineering from the School of Information Science and Technology, Dalian Maritime University, Dalian, China, in June 2022. He is a Lecturer with the School of Information Engineering, Henan Institute of Science and Technology, Xinxiang, China. His current research interests include image processing, computer vision, and machine learning.